



Tidal synchronization of close-in satellites and exoplanets. III. Tidal dissipation revisited and application to Enceladus

H. A. Folonier¹ · S. Ferraz-Mello¹ · E. Andrade-Ines¹

Received: 27 July 2017 / Revised: 4 November 2018 / Accepted: 9 November 2018 /
Published online: 6 December 2018
© Springer Nature B.V. 2018

Abstract

This paper deals with a new formulation of the creep tide theory (Ferraz-Mello in *Celest Mech Dyn Astron* 116:109, 2013—Paper I) and with the tidal dissipation predicted by the theory in the case of stiff bodies whose rotation is not synchronous but is oscillating around the synchronous state with a period equal to the orbital period. We show that the tidally forced libration influences the amount of energy dissipated in the body and the average perturbation of the orbital elements. This influence depends on the libration amplitude and is generally neglected in the study of planetary satellites. However, they may be responsible for a 27% increase in the dissipation of Enceladus. The relaxation factor necessary to explain the observed dissipation of Enceladus ($\gamma = 1.2\text{--}3.8 \times 10^{-7} \text{ s}^{-1}$) has the expected order of magnitude for planetary satellites and corresponds to the viscosity $0.6\text{--}1.9 \times 10^{14} \text{ Pa s}$, which is in reasonable agreement with the value recently estimated by Efroimsky (*Icarus* 300:223, 2018) ($0.24 \times 10^{14} \text{ Pa s}$) and with the value adopted by Roberts and Nimmo (*Icarus* 194:675, 2008) for the viscosity of the ice shell ($10^{13}\text{--}10^{14} \text{ Pa s}$). For comparison purposes, the results are extended also to the case of Mimas and are consistent with the negligible dissipation and the absence of observed tectonic activity. The corrections of some mistakes and typos of paper II (Ferraz-Mello in *Celest Mech Dyn Astron* 122:359, 2015) are included at the end of the paper.

This article is part of the topical collection on Close Approaches and Collisions in Planetary Systems.
Guest Editors: Rudolf Dvorak, Christoph Lhotka and Alessandra Celletti.

Electronic supplementary material The online version of this article (<https://doi.org/10.1007/s10569-018-9872-2>) contains supplementary material, which is available to authorized users.

✉ S. Ferraz-Mello
sylvio@iag.usp.br

H. A. Folonier
folonier@usp.br

E. Andrade-Ines
eandrade.ines@gmail.com

¹ Instituto de Astronomia Geofísica e Ciências Atmosféricas, Universidade de São Paulo, São Paulo, Brasil

1 Introduction

The calculus of the energy dissipation inside a stiff body is generally done by estimating the dissipation resulting from the action of the primary tidal force in deforming the planet (Kopal 1963; Kaula 1963, 1964; Peale and Cassen 1978; Segatz et al. 1988; Wisdom 2008; Shoji et al. 2013; Frouard and Efroimsky 2017). Such approach involves the choice of the physical model of the forces acting on the body at the microscopic level and of the dissipation parameters inside the body. An indirect approach was discussed by Kaula (1964, p. 677) in which the bulk dissipation is calculated from the estimation of the total mechanical energy lost by the system. This approach was used by Yoder and Peale (1981) to estimate the tidal energy dissipated in a synchronous satellite, by Lissauer et al. (1984) to study the melting of Enceladus, by Ferraz-Mello et al. (2009) and Ferraz-Mello (2013) to estimate the energy dissipated in the frame of Darwin's and creep tide theories, respectively, and by Correia et al. (2014) in the frame of a Maxwell model.

In this paper, we revisit the indirect approach to evaluate the bulk loss of mechanical energy by the system. This approach has the merit of its simplicity. If the companion body (the body responsible for the tide raised in the stiff body) is considered as a mass point, the energy tidally dissipated in the primary body (the stiff body under consideration) may only take origin in its rotation and in the orbit of the system. The secular variations of the semimajor axis and of the rotation of the body are the two gauges allowing us to evaluate the mechanical energy lost by the system. No other non-primeval source exists able to continuously add energy to the system. We thus consider the energy exchanged with the orbit due to the direct attraction of the two bodies, the stored rotational energy in the primary body. Several minor contributions, considered for the sake of completeness, are shown to be negligible.

We remind that the only assumption of the adopted tide theory is that self-gravitation and tidal stress permanently adjust the surface of the body to an equilibrium surface with speed given by the Newtonian creep law. The adjustment is ruled by an approximate solution of the Navier–Stokes equation for the flow of matter in the immediate neighborhood of the equilibrium surface of the body. No constitutive equation linking strain and stress is introduced at any point in the creep tide theory. All developments to reach the conclusion are the solution of the creep differential equation and the use of classical Physics to compute the force and torque acting on the companion due to the tidal deformation of the primary. The observed dissipation law results directly from the above described first principles of Physics, with approximations, but no additional ad hoc hypotheses. However, the integration of the basic equation of the creep tide theory in papers I and II assumes that the rotation of the body and the Keplerian elements of the orbit do not show significant variations in one orbital period. In the case of stiff bodies with a nearly synchronous rotation, however, it has been shown that the rotation of the bodies is not damped to a stationary value (as gaseous bodies) but is rather driven to a periodic attractor with the same period as the orbital motion and amplitude proportional to the orbital eccentricity (see Correia et al. 2014; Ferraz-Mello 2015; Folonier 2016).¹ Consequently, in such case, this physical libration needs to be considered in the integration of the basic differential equation of the creep. In this way, we propose a new model for the classical theory, assuming that the shape of the tidally deformed body may be approximated by a triaxial ellipsoid, where its flattenings and orientation are unknown functions of the time. (This idea is supported by the analytical solutions of the creep equation

¹ This forced libration is related to the asymmetries of the tides raised on the body; it is different from the asymmetries resulting from the assumption of a permanent triaxiality of the body (see Frouard and Efroimsky 2017).

given in papers I and II.) Then, the creep equation allows us to find the differential equations that describe the time evolution of this ellipsoidal bulge and its orientation, resulting in a very simpler and compact approach.

The results are applied to Enceladus and Mimas. These satellites are selected for this study because of the amount of observational information available. We know from Cassini's observations the second-degree components of the gravitational field (Iess et al. 2014). We also know that the crust of Enceladus presents a forced libration of $0.120^\circ \pm 0.014^\circ$ (Thomas et al. 2016) and that a huge quantity of heat flows from the satellite (5–16 GW cf Howett et al. 2011; Spencer et al. 2013; Le Gall et al. 2017). In contrast, Mimas presents a larger forced libration of $0.838^\circ \pm 0.002^\circ$ (Tajeddine et al. 2014) and the absence of current tectonic activity is evidence of a small dissipation (smaller than 1 GW). In addition, in both cases the three radii of the best ellipsoid representing the satellite surface are known (see Archinal et al. 2018).

The presence of the physical libration affects the dissipation increasing it, but the increase is not so important as to affect the order of magnitude of the dissipation and certainly not so important as some preliminary results of this investigation seemed to indicate. The amount of dissipation observed by Cassini corresponds to a relaxation factor in the range $\gamma = 1.2\text{--}3.8 \times 10^{-7} \text{ s}^{-1}$ for Enceladus and $\gamma \sim 10^{-9} \text{ s}^{-1}$ for Mimas. The difference between these values is consistent with the fact that the gravitational acceleration at the surface and the density are both much larger in Enceladus than in Mimas. On the other hand, these values of relaxation factors indicate a viscosity $\eta = 0.6\text{--}1.9 \times 10^{14} \text{ Pa s}$ for Enceladus and $\eta \sim 10^{16} \text{ Pa s}$ for Mimas. This estimation for the Enceladus viscosity has the same order as the value recently estimated by Efroimsky (2018) ($0.24 \times 10^{14} \text{ Pa s}$) and as the value adopted by Roberts and Nimmo (2008) for the viscosity of the ice shell ($10^{13}\text{--}10^{14} \text{ Pa s}$). It is also close to the reference viscosity of water at 255 K (10^{15} Pa s) adopted by Běhouňková et al. (2012) in their modeling of the melting events at origin of the south-pole activity on Enceladus. More recent research carried out by Čadek et al. (2019) demonstrates that the viscosity of ice at the melting temperature may be equal to or higher than $3 \times 10^{14} \text{ Pa s}$, for the ice shell to remain stable.

The forced libration obtained with the creep tide theory for homogeneous bodies, in the case of Enceladus, is 3.1 times smaller than the libration amplitude obtained from Cassini's observations. However, results close to the observation were obtained in a preliminary extension of the core-shell model developed by the authors (Folonier 2016; Folonier and Ferraz-Mello 2017, Folonier et al., in preparation), in which one liquid layer is assumed to exist between the crust and the core.

In the found range of values of γ , the contribution of the satellite tides to the variations of the semimajor axis and eccentricity of Enceladus are $\langle \dot{a} \rangle = -(0.4\text{--}1.3) \times 10^{-5} \text{ km/y}$ and $\langle \dot{e} \rangle = -(1.9\text{--}6.0) \times 10^{-9} \text{ y}^{-1}$. The eccentricity variation is very small. Nonetheless, in the case of Enceladus, we need to consider the effects of the almost 2:1 resonance between Enceladus and Dione that produces a forced eccentricity of 0.00459 (see Ferraz-Mello 1985; Vienne and Duriez 1995). In the case of Mimas, we have found that the variations of the semimajor axis and eccentricity are $\langle \dot{a} \rangle \sim -10^{-6} \text{ km/y}$ and $\langle \dot{e} \rangle \sim -10^{-10} \text{ y}^{-1}$. In both cases, the variations found are much smaller than those due to the tides on the planet.

This paper is organized as follows: We first proceed, in Sects. 2–4, to a revisit of the creep tide theory proposing a new approach in which the differential equations for the tidal deformation of the primary, and for its rotation, are integrated simultaneously. Then, in Sect. 5, we study the case in which the rotation of the primary is nearly synchronous but not uniform showing a forced libration. In Sects. 6 and 7, we do an inventory of the main mechanical processes involving the storage of mechanical energy in the system and discuss

the law ruling the dissipation in stiff satellites, with application to Enceladus. In Sect. 8, we extend the results to obtain the average variations of the metrical elements of the orbit: semimajor axis and eccentricity. In the final sections, we extend the results to Mimas and present the conclusions. The paper is completed by two appendices, where are given some technical details of the model used to evaluate the orbital energy (“Appendix 1”) and the analytical approximation of the spin-orbit quasi-synchronous attractor (“Appendix 2”). In addition, an Online Supplement is provided, where the classical creep tide approach is also extended to include the near-synchronous, but not uniform, rotation case.

2 The creep tide equations

Let us consider one system formed by the extended body m (primary) and the mass point M (companion), and let \mathbf{r} be the radius vector in a system of reference centered on m . We assume that the primary is a homogeneous body and have an angular velocity of rotation $\boldsymbol{\Omega}$, perpendicular to the orbital plane.

In the creep tide theory, the tidal deformation of m is obtained by solving the Newtonian creep law

$$\dot{\zeta} = \gamma(\rho - \zeta), \tag{1}$$

where γ is the relaxation factor (see paper I), $\zeta = \zeta(\widehat{\varphi}, \widehat{\theta}, t)$ is the distance of the surface point of coordinates $\widehat{\varphi}$ (longitude) and $\widehat{\theta}$ (co-latitude) to the center of gravity of the body, and $\rho = \rho(\widehat{\varphi}, \widehat{\theta}, t)$ is the surface of the static figure of equilibrium of m under the gravitational attraction of M . ρ is approximated by a triaxial ellipsoid whose major axis is oriented toward M , and whose equatorial prolateness and polar oblateness are

$$\epsilon_\rho = \frac{a - b}{R_e} = \frac{15MR_e^3}{4mr^3}, \tag{2}$$

and

$$\epsilon_z = 1 - \frac{c}{R_e} = \frac{\epsilon_\rho}{2} + \frac{5\Omega^2 R_e^3}{4Gm}, \tag{3}$$

where a, b, c are the semimajor axes of the triaxial ellipsoid, R_e is the mean equatorial radius, G is the gravitational constant, and Ω is the spin rate of m (see Tisserand 1891; Choblet et al. 2017; Folonier et al. 2015). Its equation is²

$$\rho(\widehat{\theta}, \widehat{\varphi}, t) = R \left(1 + \frac{1}{2}\epsilon_\rho \sin^2 \widehat{\theta} \cos(2\widehat{\varphi} - 2\varphi) + \epsilon_z \left(\frac{1}{3} - \cos^2 \widehat{\theta} \right) \right), \tag{4}$$

where φ is the true longitude of the companion in its equatorial orbit around the primary and R is the mean radius of the primary. The angles are such that the major axis of the ellipsoid is always oriented toward the companion (*left* panel of Fig. 1). The right-hand side is a time function depending on the longitude $\widehat{\varphi}$ (such that $d\widehat{\varphi}/dt = \Omega(t)$) and on the polar coordinates of the companion, r and φ . The radius vector of M , r , is introduced in the equation by the flattenings ϵ_ρ and ϵ_z .

In previous papers (papers I and II) the forced terms in the solution of Eq. (1) were approximated by the sum of an arbitrary number of ellipsoidal bulges over one sphere of

² In paper II (Ferraz-Mello 2015), the variation of R_e has been neglected. However, when the equatorial prolateness varies due to a variation in the distance of m to M , the polar flattening and R_e vary accordingly: $R_e \simeq R(1 + \frac{1}{3}\epsilon_z)$ where R is the mean radius of the primary (constant).

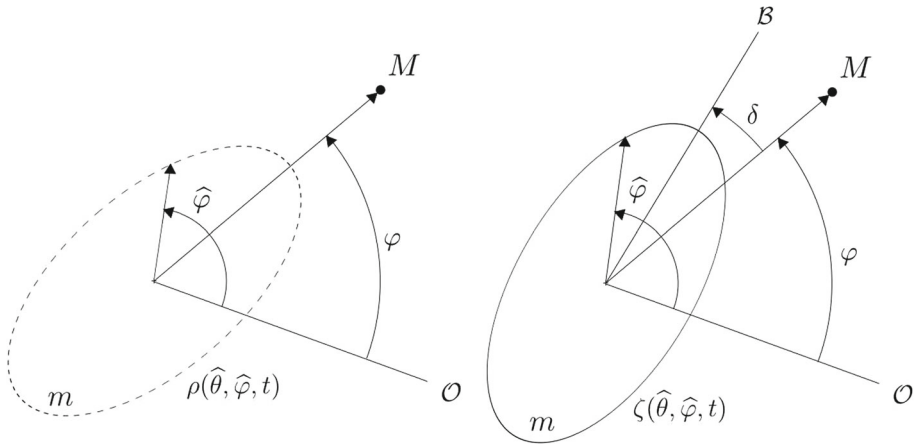


Fig. 1 Equatorial sections of the ellipsoids $\rho(\hat{\theta}, \hat{\varphi}, t)$ and $\zeta(\hat{\theta}, \hat{\varphi}, t)$ corresponding to the tide on m generated by M . Angles: φ and $\hat{\varphi}$ are the longitudes, in a fixed reference system, of the companion and of one point on the surface of the primary, respectively. δ is the orientation angle of the tidal bulge (labeled B) with respect to the companion

radius R (see papers I and II), where each bulge has different flattenings and orientation. To the first order in the flattenings, the sum of two or more ellipsoidal bulges can be expressed by a new ellipsoidal bulge with its flattenings and orientation (see ‘‘Appendix 3’’ of Folonier and Ferraz-Mello 2017). For this reason, ζ can be approximated by a homogeneous ellipsoid:

$$\zeta(\hat{\theta}, \hat{\varphi}, t) = R \left(1 + \frac{1}{2} \mathcal{E}_\rho \sin^2 \hat{\theta} \cos(2\hat{\varphi} - 2\varphi_B) + \mathcal{E}_z \left(\frac{1}{3} - \cos^2 \hat{\theta} \right) \right), \quad (5)$$

where the instantaneous flattenings \mathcal{E}_ρ , \mathcal{E}_z and the orientation longitude of the bulge $\varphi_B = \varphi + \delta$ are unknown functions of the time. Here, δ is the orientation angle of the bulge vertex with respect to M (right panel of Fig. 1).

In order to find the time evolution of these unknown functions, we differentiate (5) with respect to the time and replace the result into the creep Eq. (1). We obtain:

$$\begin{aligned} & \left((\dot{\mathcal{E}}_\rho + \gamma \mathcal{E}_\rho) \cos 2\delta + \mathcal{E}_\rho (2\Omega - 2\dot{\varphi} - 2\dot{\delta}) \sin 2\delta \right) \frac{1}{2} R \sin^2 \hat{\theta} \cos(2\hat{\varphi} - 2\varphi) \\ & + \left(-\mathcal{E}_\rho (2\Omega - 2\dot{\varphi} - 2\dot{\delta}) \cos 2\delta + (\dot{\mathcal{E}}_\rho + \gamma \mathcal{E}_\rho) \sin 2\delta \right) \frac{1}{2} R \sin^2 \hat{\theta} \sin(2\hat{\varphi} - 2\varphi) \\ & + R (\dot{\mathcal{E}}_z + \gamma \mathcal{E}_z) \left(\frac{1}{3} - \cos^2 \hat{\theta} \right) = \frac{1}{2} R \sin^2 \hat{\theta} \gamma \mathcal{E}_\rho \cos(2\hat{\varphi} - 2\varphi) + R \gamma \mathcal{E}_z \left(\frac{1}{3} - \cos^2 \hat{\theta} \right). \end{aligned} \quad (6)$$

Since the flattenings \mathcal{E}_ρ , \mathcal{E}_z and the angle of orientation δ cannot depend on one specific point on the surface of m (that is $\hat{\theta}$, $\hat{\varphi}$), we can decompose Eq. (6) into three equations, one for each trigonometric argument, which may be written as

$$\begin{aligned} \dot{\delta} &= \Omega - \dot{\varphi} - \frac{\gamma \mathcal{E}_\rho}{2\mathcal{E}_\rho} \sin 2\delta \\ \dot{\mathcal{E}}_\rho &= \gamma (\mathcal{E}_\rho \cos 2\delta - \mathcal{E}_\rho) \\ \dot{\mathcal{E}}_z &= \gamma (\mathcal{E}_z - \mathcal{E}_z). \end{aligned} \quad (7)$$

This system of differential equations of first order allows us to calculate the time evolution of the instantaneous flattenings and the instantaneous orientation angle, when the orbital motion of the companion (that is, r and $\dot{\varphi}$) and the spin rate Ω are known. This new version of the creep equations is formally analogous to the one used by Correia et al. (2014), Boué et al. (2016), Correia et al. (2018) and Beaugé (personal communication).

3 The disturbing potential

The disturbing potential created by the homogeneous triaxial ellipsoid m , the bulge of which is rotated of an angle φ_B with respect to the axis x , at the companion $M(r, \theta = \pi/2, \varphi)$, neglecting the harmonics of degree higher than 2, is:

$$\delta U(\mathbf{r}) = -\frac{G(B-A)}{2r^3} (3 \cos^2 \Psi_B - 1) - \frac{G(C-B)}{2r^3}, \quad (8)$$

where G is the gravitational constant, Ψ_B is the angle between the direction of the point where the potential is taken and the direction of the bulge vertex, labeled by B (see Fig. 1), and A, B, C are the moments of inertia of the ellipsoid with respect to its principal axes ($A < B < C$).

The cosine can be written as

$$\cos \Psi_B = \hat{\mathbf{r}} \cdot \hat{\mathbf{r}}_B, \quad (9)$$

where $\hat{\mathbf{r}}$ and $\hat{\mathbf{r}}_B$ are the unitary vectors oriented toward the companion and the bulge direction, respectively. The differences $B - A$ and $C - B$, to the first order in the flattenings, can be approximated by

$$B - A \approx C \mathcal{E}_\rho; \quad C - B \approx C \left(\mathcal{E}_z - \frac{1}{2} \mathcal{E}_\rho \right). \quad (10)$$

The moment of inertia with respect to the polar axis is $C = m(a^2 + b^2)/5$ or, introducing the flattenings of the ellipsoid resulting from the integration of the creep differential equation

$$C = \frac{2}{5} m R^2 \left(1 + \frac{2}{3} \mathcal{E}_z + \mathcal{O}(\mathcal{E}^2) \right). \quad (11)$$

Hence, using the definition of ϵ_ρ , the resulting disturbing potential is

$$\delta U(\mathbf{r}) = -\frac{2Gm^2\epsilon_\rho}{25MR} \mathcal{E}_\rho \left(2(\hat{\mathbf{r}} \cdot \hat{\mathbf{r}}_B)^2 - 1 \right) - \frac{4Gm^2\epsilon_\rho}{75MR} \mathcal{E}_z. \quad (12)$$

It is important to emphasize that, since the beginning of this paper, we have used the same notation \mathbf{r} to indicate the radius vector of the companion in all situations. We have thus broken with the tradition of using \mathbf{r}^* (or \mathbf{r}') to indicate the radius vector of the companion in the equations used to calculate the tidal deformation of the primary (Darwin 1880; Kaula 1964; MacDonald 1964; Efroimsky 2012). The dichotomy \mathbf{r}, \mathbf{r}^* was introduced by Darwin for the only reason that, in the calculus of the force as the gradient of the potential U , the derivatives of the potential must be done with respect to the coordinates of the mass point where the force is applied. Thus, it was important to use a different notation for the radius vector and its components in the calculation of the flattenings, and to write the potential as a function $U(\mathbf{r}, \mathbf{r}^*)$ making explicit which of the radii vectors was to be considered when the force is calculated. But, physically, there is only one radius vector being considered and, after the gradient calculation, \mathbf{r} and \mathbf{r}^* are identified. As in Correia et al. (2014), Boué et al.

(2016), Ragazzo and Ruiz (2017) and Correia et al. (2018), in the approach proposed in this paper, the potential does not depend explicitly on both instances of the radius vector. The radius vector used in the calculation of the flattenings is substituted by the time functions \mathcal{E}_ρ and \mathcal{E}_z , and the only radius vector \mathbf{r} appearing in Eq. (7) is the radius vector of the point where the force is being applied.

4 The tidal force and torque

To calculate the tidal force \mathbf{F} acting on the mass M located in M , we take the negative gradient of the disturbing potential of m and multiply it by the mass placed in the point. Hence

$$\mathbf{F} = -M\nabla_{\mathbf{r}}\delta U. \tag{13}$$

The sign in this expression comes from the fact that we are using the conventions of Physics (δU is a potential not a force function). It is important to stress that in agreement with Newton laws, there exists a reaction force $-\mathbf{F}$ acting on m due to the attraction of M (see Ferraz-Mello et al. 2003). This fact is generally neglected in studies where one of the masses is negligible when compared to the other but its neglect in general problems is an error. Then, we obtain:

$$\mathbf{F} = -\frac{2Gm^2\epsilon_\rho}{25Rr^2}\mathcal{E}_\rho\left(10(\hat{\mathbf{r}}\cdot\hat{\mathbf{r}}_B)^2\mathbf{r} - 4r(\hat{\mathbf{r}}\cdot\hat{\mathbf{r}}_B)\hat{\mathbf{r}}_B - 3\mathbf{r}\right) - \frac{4Gm^2\epsilon_\rho}{25Rr^2}\mathcal{E}_z\mathbf{r}. \tag{14}$$

The unitary vector $\hat{\mathbf{r}}_B$ can be decomposed in terms of the unitary vectors $\hat{\mathbf{r}}$ and $(\hat{\mathbf{z}}\times\hat{\mathbf{r}})$, where $\hat{\mathbf{r}}$ and $\hat{\mathbf{z}}$ are the unitary vectors oriented toward M and along the z -axis, respectively:

$$\hat{\mathbf{r}}_B = \cos\delta\hat{\mathbf{r}} + \sin\delta(\hat{\mathbf{z}}\times\hat{\mathbf{r}}). \tag{15}$$

Hence, the resulting tidal force acting on M can be written as:

$$\mathbf{F} = -\frac{2Gm^2\epsilon_\rho}{25Rr^2}\mathcal{E}_\rho\left(3\cos 2\delta\mathbf{r} - 2\sin 2\delta(\hat{\mathbf{z}}\times\mathbf{r})\right) - \frac{4Gm^2\epsilon_\rho}{25Rr^2}\mathcal{E}_z\mathbf{r}. \tag{16}$$

Finally, the tidal torque acting on M is $\mathbf{M} = \mathbf{r}\times\mathbf{F}$, or:

$$\mathbf{M} = \frac{4Gm^2\epsilon_\rho}{25R}\mathcal{E}_\rho\sin 2\delta\hat{\mathbf{z}}. \tag{17}$$

It is important to note that, in order to calculate the angular acceleration of the primary, we need to consider the reaction on the primary, that is

$$-\mathbf{M} = C\dot{\Omega} + \dot{C}\Omega, \tag{18}$$

where the time variation of the axial moment of inertia is

$$\dot{C} \approx \frac{4}{15}mR^2\dot{\mathcal{E}}_z. \tag{19}$$

We note that, at this order of approximation, the equatorial tidal prolateness does not affect the moment of inertia (the deformations inward and outward compensate themselves).

The scheme considered in this approach differs from the scheme used in papers I and II. Here, the equations of the instantaneous ellipsoidal bulge and its orientation may be integrated together with the rotational equation, while, in papers I and II, the shape of the primary is calculated assuming Ω as a known time function through the longitude $\hat{\varphi} = \Omega(t - t_0)$. Once the shape has been determined, it is used to obtain the rotational evolution of the deformed body.

The model presented here allows us also to calculate the orbital evolution of the companion, as well as the evolution of the ellipsoidal bulge, its orientation and the rotational evolution of the primary. However, in general, the variation of the orbital elements is much slower and, for short time spans, we may assume a Keplerian motion for the companion. The instantaneous shape, orientation and rotation of the primary are then calculated using Eqs. (7) and (17) and the classical two-body expressions for r and $\dot{\phi}$.

5 Solution in the neighborhood of the synchronous rotation

In the neighborhood of the synchronization, the rotation of close-in satellites and exoplanets is generally damped toward a final stable state which depends on the nature of the body. The rotation of gaseous planets, of fast relaxation (high γ , low viscosity), tends to a stationary rotation slightly faster than the orbital motion (a.k.a. supersynchronous motion). The excess of angular velocity is $\sim 6ne^2$ (see paper I). On the other end, the rotation of planetary satellites and Earth-like planets, of slow relaxation (low γ , high viscosity), is damped to attractors with the same period as the orbital period and the final rotations are not uniform. They are forced oscillations (physical librations) around one center. In this case, the solution of the creep equation can no longer be calculated as in papers I and II. The use of the uniform approximation for Ω is no longer appropriate because the rotation is, in this case, affected by a significant short-period oscillation.³ It is important to emphasize that in the approach adopted in this paper, no hypotheses on the rotation behavior are necessary since all equations are integrated simultaneously. The synchronous attractor may be approximated by

$$v \stackrel{\text{def}}{=} 2(\Omega - n) \cong B_0 + B_1 \cos \ell + B_2 \sin \ell, \quad (20)$$

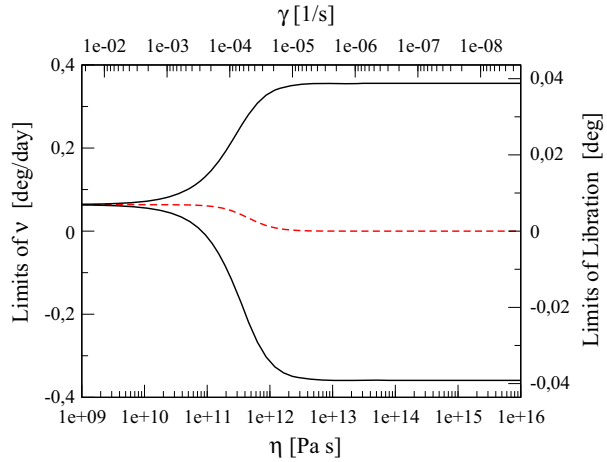
where ℓ is the mean anomaly of the companion; the mean value B_0 and the amplitudes B_1 , B_2 are constants (for the details of the calculation of the synchronous attractor, see “Appendix 2”).

In the case of Enceladus, the numerical solution of the exact equations for low values of γ is an almost symmetric oscillation of v . The semi-amplitude of this oscillation depends on the adopted relaxation factor (see Fig. 2). If $\gamma < 10^{-5} \text{ s}^{-1}$, the forced oscillation amplitude is 0.36 deg/d.

This value may be compared to the observed values (see Table 2). Measurements of control points on the surface of Enceladus accumulated over seven years of Cassini’s observations allowed Thomas et al. (2016) to determine the satellite’s rotation state. They have found a libration of $0.120^\circ \pm 0.014^\circ$. If we assume that these oscillations follow a harmonic law we obtain, correspondingly, for the oscillation of the velocity of rotation: $0.56 \pm 0.06 \text{ deg/day}$, and for the semidiurnal frequency $1.12 \pm 0.12 \text{ deg/day}$. The immediate conclusion from the comparison of these values is that it is not possible to reproduce exactly the observed forced libration of Enceladus with a homogeneous body model. The predicted oscillation is smaller. However, results close to the observation were obtained in a preliminary extension of the core-shell model developed by the authors, when one liquid layer is assumed to exist between the crust and the core (Folonier 2016; Folonier and Ferraz-Mello 2017, Folonier et al., in preparation).

³ The extension of the theory of papers I and II to the case in which the rotation is trapped in a periodic attractor is given in the Online Supplement linked to this paper.

Fig. 2 Tidal forced oscillation of the semidiurnal frequency of one body like Enceladus in function of the viscosity η and the relaxation factor γ (shown on the upper axis). The black lines are the limits of the oscillation. The red dashed line is the mean value of ν . In the right axis we show the corresponding limit of the physical libration when a harmonic oscillation is assumed



For the sake of comparison, we may note that viscoelastic models adopting a permanent triaxiality give a result yet smaller: $\lesssim 0.03$ deg depending on the adopted triaxiality (Rambaux et al. 2010).

6 The energy balance

In this section, we examine the various manifestations of the mechanical energy in a system formed by two mutually attracting bodies: the extended body m and one mass point M . Let their masses be, respectively, m and M . We consider only the case where M lies on the equatorial plane of m . Our aim is to evaluate the amount of the energy dissipated by the body.⁴

Let us first review some known facts of a system formed by the extended body m and the mass point M (see Scheeres 2002). Let \mathbf{r} , \mathbf{V} be the radius vector and the velocity of M in a system of reference centered on m . The kinetic energy referred to the center of gravity of the system formed by the two bodies and the rotational energy of M are

$$E_{\text{kin}} = \frac{1}{2} \frac{Mm}{M+m} \mathbf{V}^2; \quad E_{\text{rot}} = \frac{1}{2} C \Omega^2, \tag{21}$$

the time-dependent gravitational potential generated by the primary in the point \mathbf{r} is

$$MU(\mathbf{r}; t) = -\frac{GMm}{r} - \frac{2Gm^2}{25R} \left(\epsilon_\rho \mathcal{E}_\rho \cos(2\varphi - 2\varphi_B) - \frac{2}{3} \epsilon_\rho \mathcal{E}_z \right), \tag{22}$$

and E_{int} is the internal gravitational energy of the primary. Using the explicit formulas given by Essén (2004) (see “Appendix 1”), we obtain

$$E_{\text{int}} = -\frac{3Gm^2}{5R} \left(1 - \frac{1}{15} \mathcal{E}_\rho^2 - \frac{4}{45} \mathcal{E}_z^2 \right). \tag{23}$$

⁴ The dissipation in each one of the two bodies may be considered separately. Within the order of approximation generally adopted (first order in the tidal deformations), the variation of the energy can be split into two parts, each one associated with the tidal deformation in one of the bodies while the other—source of the tidal potential—is kept as a mass point. Therefore, only the dissipation in one of the two bodies need to be explicitly considered.

The time derivatives of the energies are

$$\dot{E}_{\text{kin}} = \frac{Mm}{M+m} \mathbf{V} \cdot \dot{\mathbf{V}} = \mathbf{f} \cdot \mathbf{V}; \quad \dot{E}_{\text{rot}} = -\mathbf{M} \cdot \boldsymbol{\Omega} - \frac{1}{2} \dot{C} \Omega^2 \tag{24}$$

(since in Newton’s law the acceleration must be referred to the barycenter, that is, $\mathbf{f} = \frac{Mm}{M+m} \dot{\mathbf{V}}$)

$$M\dot{U} = M \text{grad}_{\mathbf{r}} U \cdot \mathbf{V} + M \frac{\partial U}{\partial t} = -\mathbf{f} \cdot \mathbf{V} + M \frac{\partial \delta U}{\partial \varphi_B} \dot{\varphi}_B + M \frac{\partial \delta U}{\partial \mathcal{E}_\rho} \dot{\mathcal{E}}_\rho + M \frac{\partial \delta U}{\partial \mathcal{E}_z} \dot{\mathcal{E}}_z, \tag{25}$$

and

$$\dot{E}_{\text{int}} = \frac{\partial E_{\text{int}}}{\partial \mathcal{E}_\rho} \dot{\mathcal{E}}_\rho + \frac{\partial E_{\text{int}}}{\partial \mathcal{E}_z} \dot{\mathcal{E}}_z. \tag{26}$$

Hence,

$$\dot{E}_{\text{tot}} = \dot{E}_{\text{kin}} + M\dot{U} + \dot{E}_{\text{int}} + \dot{E}_{\text{rot}}, \tag{27}$$

or

$$\dot{E}_{\text{tot}} = M \frac{\partial \delta U}{\partial \varphi_B} \dot{\varphi}_B + M \frac{\partial \delta U}{\partial \mathcal{E}_\rho} \dot{\mathcal{E}}_\rho + M \frac{\partial \delta U}{\partial \mathcal{E}_z} \dot{\mathcal{E}}_z + \frac{\partial E_{\text{int}}}{\partial \mathcal{E}_\rho} \dot{\mathcal{E}}_\rho + \frac{\partial E_{\text{int}}}{\partial \mathcal{E}_z} \dot{\mathcal{E}}_z + \dot{E}_{\text{rot}}, \tag{28}$$

that is, the energy variation associated with the power $\mathbf{f} \cdot \mathbf{V}$ is exchanged with the kinetic energy and cannot account for the dissipation of the system energy [see Eqs. (24) and (25)]. This is a well-known fact in the study of the motion of satellites around non-spherical rigid bodies.⁵

Using Eq. (7), the time derivative of the total mechanical energy can be written as

$$\dot{E}_{\text{tot}} = -\frac{6}{5} \frac{Gm^2}{\gamma R} \left(\frac{1}{15} \dot{\mathcal{E}}_\rho^2 + \frac{1}{15} \mathcal{E}_\rho^2 (2\Omega - 2\dot{\varphi} - 2\dot{\delta})^2 + \frac{4}{45} \dot{\mathcal{E}}_z^2 \right) \leq 0. \tag{29}$$

The time derivative of the total mechanical energy is always negative.

Finally, the orbital energy is:

$$E_{\text{orb}} = E_{\text{kin}} + MU(\mathbf{r}; t), \tag{30}$$

and, using Eqs. (24)–(25), the time derivative of the orbital energy is

$$\dot{E}_{\text{orb}} = \dot{E}_{\text{kin}} + M\dot{U}(\mathbf{r}; t), \tag{31}$$

This definition of the orbital energy variation is the same as adopted by Correia et al. (2014).

7 Dissipation

The actual variation of the main components of the mechanical energy is shown in the left panel of Fig. 3. It is large, indicating a great periodic energy exchange between the rotational energy (labeled *rot*) and the sum of the orbital energy and the internal gravitational energy (labeled *sum*). The amplitudes of variation of the orbital and rotational energies have the same order of magnitude and the variation of the total energy (labeled *tot* in Fig. 3), shows only a very small variation (of the order of one part in 10⁵ of the variation of the two components). This very small periodic variation of the time derivative of the total mechanical energy is always negative (right panel of Fig. 3).

⁵ It is worth stressing that we are referring to the actual energy of the system. At variance with it, the energy of the osculating Keplerian motion may vary (as well as the osculating semimajor axis) but such variation is only a consequence of the way in which osculating variables are defined.

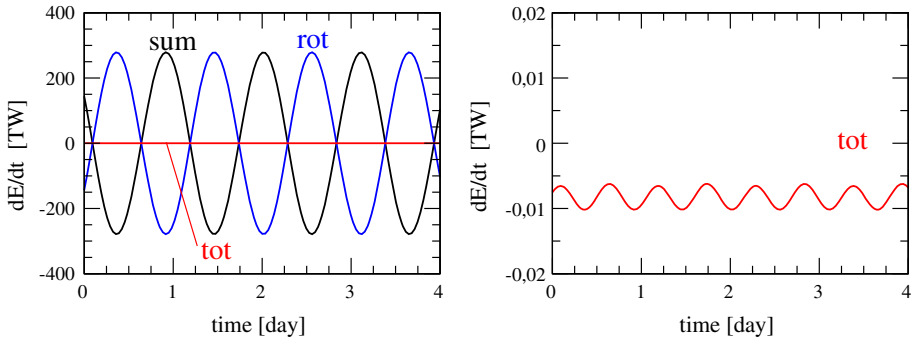


Fig. 3 Left: tidal variation of the mechanical energy (after the vanishing of the transients): the sum of the orbital energy and the internal gravitational energy (black line labeled sum), the rotational (blue line labeled rot), and the total mechanical energy (red line labeled tot). Right: \dot{E}_{tot} in a magnified scale. N.B. $\gamma = 2 \times 10^{-7} \text{s}^{-1}$

In the long run, the only sources for the energy dissipated by the tides are the orbital and the rotational energies. The usual operation to get rid of periodic variations is the averaging of the total mechanical energy. The canonical tool to separate conservative and dissipative terms is the analysis of the differential form expressing the variation of the orbital energy. However, in the adopted model, only the attraction of the external body M by the deformed body m is available. The dynamics of the action of M creating the deformation in m is concealed by the creep equation used to determine the shape of m . The averaging to zero of the periodic variations may be considered as the equivalent of the zero variation of the energy on a closed path characteristic of the conservative phenomena.

7.1 Analytical approximation

The variable characterizing the variation in a short time interval is the mean anomaly ℓ , and the averaging operation is just $\frac{1}{2\pi} \int_0^{2\pi} \dot{E}_{tot} d\ell$. In the case of Enceladus, the result is shown in Fig. 4. We note that the resulting $\langle \dot{E}_{tot} \rangle = \langle \dot{E}_{orb} + \dot{E}_{rot} + \dot{E}_{int} \rangle$ (black solid line) is negative, hence, the system is losing mechanical energy, as expected. Using the analytical solution detailed in ‘‘Appendix 2,’’ the time average of the total mechanical energy (given by Eq. 29), for the synchronous attractor, can be approximated as

$$\langle \dot{E}_{tot} \rangle_{sync} = -\frac{21GMmR^2\bar{\epsilon}_\rho e^2}{5a^3} \frac{n^2\gamma}{n^2 + \gamma^2}, \tag{32}$$

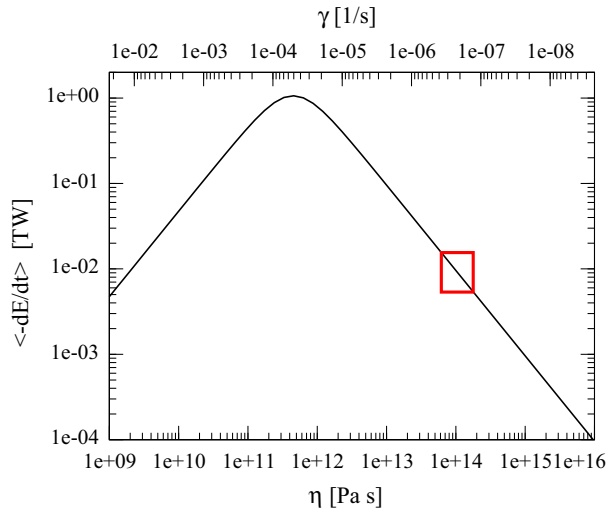
to the first order in the flattenings.

For sake of completeness, it is worth repeating some properties of this result: (1) the result is always negative (energy is lost); (2) the variation of the dissipation with the relaxation factor has the inverted V-shape, characteristic of the Maxwell rheology; (3) in the neighborhood of the stationary solution, the quantity defined by Eq. (32) is of the order $\mathcal{O}(e^2)$.

In the case of Enceladus, the estimations of the heat dissipated in the SPT (south polar terrain) area based on the observations with Cassini are in the range 5–16 GW (cf Howett et al. 2011; Spencer et al. 2013; Le Gall et al. 2017). This observed dissipation corresponds to a relaxation factor $\gamma = 1.2\text{--}3.8 \times 10^{-7} \text{ s}^{-1}$ (red box in Fig. 4). The viscosity corresponding to this relaxation⁶ is $0.6\text{--}1.9 \times 10^{14} \text{ Pas}$. The physical libration is responsible for a 27%

⁶ According with the relation $\gamma = wR/2\eta$ given in papers I and II (w is the specific weight at the surface of the body).

Fig. 4 Dissipation curve: average of the net variation of the mechanical energy. The body and orbital parameters used correspond to a homogeneous Enceladus. The actual range of the observed dissipation and the corresponding ranges for the viscosity (and for the relaxation factor) are shown by a red box



increase in the dissipation of Enceladus (See Section 5 in the Online Supplement). This last result is in good agreement with the value 30% found by Efroimsky (2018).

8 Semimajor axis and eccentricity average perturbations

8.1 Semimajor axis

The variation of the osculating semimajor axis due to the tides raised on m may be obtained using the corresponding Lagrange variational equation:

$$\dot{a} = \frac{2}{na} \frac{\partial \mathcal{R}}{\partial \ell}, \tag{33}$$

where the disturbing function is $\mathcal{R} = -(1 + M/m)\delta U$ (see Brouwer and Clemence 1961, Chap. XI). The minus sign is included because δU is a potential (not a force function), and the factor $(1 + M/m)$ is introduced to account for the fact that the disturbing force is not of external origin but an interaction between the two bodies. We thus consider the force per unit mass acting on one body minus its reaction on the other body (see discussion in Ferraz-Mello et al. 2009, Section 18).

Hence, considering the third Kepler law ($n^2 a^3 = G(M + m)$) and comparing to the work calculated above,

$$\dot{a} = \frac{2a^2}{GmM} \dot{E}_{\text{orb}}. \tag{34}$$

This is the same equation obtained when taking the time derivatives of both sides of the two-body classical equation relating the orbital energy and the osculating semimajor axis, $E_{\text{orb}} = -GmM/2a$ (see Brouwer and Clemence 1961), which has been used in previous papers (see paper I). It shows that \dot{E}_{orb} is equal to the time derivative of the Keplerian orbital energy of the system.

The variation of the semimajor axis due to the tidal deformations of the primary is given by Eq. (34). The results corresponding to a homogeneous Enceladus are shown in Fig. 5

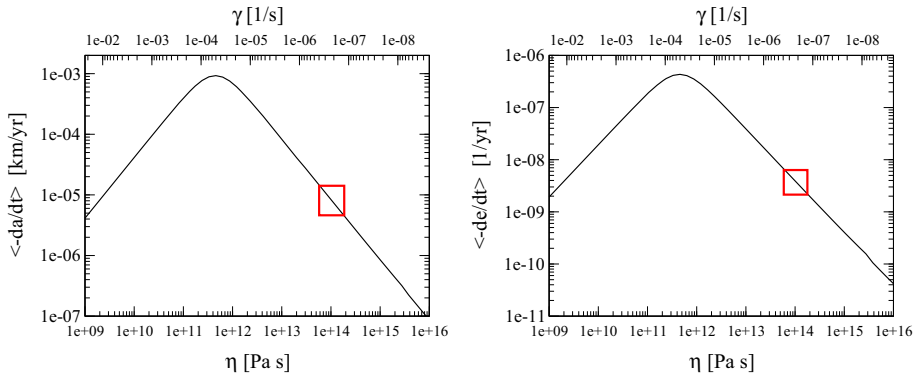


Fig. 5 Variation of the averages of $-da/dt$ (Left) and $-de/dt$ (Right) in function of the viscosity η (or γ , see the top axis) for a body like Enceladus. In each plot the red box indicates the values corresponding to the actual range of the observed dissipation of Enceladus

(Left). In that figure the average variation of da/dt is shown for a wide range of values of γ . The average has the same aspect as the dissipation law shown in Fig. 4. This similarity happens because, near the stationary solution, the dissipated energy comes almost totally from $\langle \dot{E}_{orb} \rangle$ (the average variation of rotational energy $\langle \dot{E}_{rot} \rangle$ is several orders of magnitude smaller). When $\gamma = 1.2 - 3.8 \times 10^{-7} \text{ s}^{-1}$, we obtain $\langle \dot{a} \rangle = -(0.4 - 1.2) \times 10^{-5} \text{ km/y}$ (the red box in Fig. 5 Left).

It is important to emphasize that this is not the actual rate of change of the semimajor axis. This is only the part of it due to the tides on the satellite. To obtain the actual rate of change of a , it is necessary to consider also the part of it due to the tides raised on the planet, which is given by the same equations but where the variables are interchanged to express the dissipation on the planet instead of the satellite. In the case of Enceladus, the two effects appear to have similar orders of magnitude; according to Lainey et al. (2012), the variation of the semimajor axis due to the tides raised by Enceladus on Saturn is $4.2 \times 10^{-5} \text{ km/y}$. The variation of the semimajor axis of Saturnian satellites is important for some theories of the formation of these satellites (see Lainey et al. 2012). The orbital variations due to the tides raised on the planet are more important than the variations due to the tides raised on the satellite and correspond to a present expansion of the satellite’s orbit.

8.2 Eccentricity

The variation of the eccentricity is given by the corresponding Lagrange variational equation:

$$\dot{e} = -\frac{\sqrt{1-e^2}}{na^2e} \frac{\partial \mathcal{R}}{\partial \omega} + \frac{1-e^2}{na^2e} \frac{\partial \mathcal{R}}{\partial \ell}, \tag{35}$$

(see Brouwer and Clemence 1961). This equation is equivalent to

$$\dot{e} = \frac{1-e^2}{e} \left(\frac{\dot{a}}{2a} - \frac{\dot{\mathcal{L}}}{\mathcal{L}} \right), \tag{36}$$

where $\mathcal{L} = \frac{GMm}{na} \sqrt{1-e^2}$ is the orbital angular momentum. In order to use the averages given in the previous sections, we may introduce a change in this equation reminding that $\dot{\mathcal{L}} = M_z = -\dot{E}_{rot}/\Omega$. Hence

$$\langle \dot{e} \rangle = \frac{1 - e^2}{e} \left(\frac{\langle \dot{a} \rangle}{2a} + \frac{1}{\mathcal{L}} \left\langle \frac{\dot{E}_{\text{rot}}}{\Omega} \right\rangle \right). \quad (37)$$

The variation of the averaged de/dt as a function of the relaxation factor γ is shown in Fig. 5 (Right). When $\gamma = 1.2\text{--}3.8 \times 10^{-7} \text{ s}^{-1}$, the averages are very small (less than 10^{-10} y^{-1}). In general, the eccentricity variation may become important in long-term studies but, in the case of Enceladus, the effects of the almost 2:1 resonance between Enceladus and Dione produces a forced eccentricity of 0.00459 that must be considered (see Ferraz-Mello 1985; Vienne and Duriez 1995). We remind that the proper eccentricity of Enceladus is only 0.00012.

8.3 Analytical approximations

Proceeding similarly to the previous section, the average of the variation of the osculating semimajor axis due to the tide in the primary can be approximated, in the neighborhood of the synchronous rotation, as

$$\langle \dot{a} \rangle_{\text{sync}} = \frac{2a^2}{GMm} \langle \dot{E}_{\text{tot}} \rangle_{\text{sync}} = -\frac{42R^2 \bar{\epsilon}_\rho e^2}{5a} \frac{n^2 \gamma}{n^2 + \gamma^2}, \quad (38)$$

and the approximation of the average of the variation of the osculating eccentricity, in the neighborhood of the synchronous rotation, is

$$\langle \dot{e} \rangle_{\text{sync}} = \frac{1 - e^2}{2ae} \langle \dot{a} \rangle_{\text{sync}} = -\frac{21R^2 \bar{\epsilon}_\rho e(1 - e^2)}{5a^2} \frac{n^2 \gamma}{n^2 + \gamma^2}. \quad (39)$$

In both cases, the averages vanish when $e \rightarrow 0$. We may easily see that, when the quasi-synchronous rotation is assumed, both $\langle da/dt \rangle$ as $\langle de/dt \rangle$ become proportional to $\langle \dot{E}_{\text{tot}} \rangle_{\text{sync}}$.

9 Extension to Mimas

One challenge to every theory for the dissipation of the Enceladus is that it shall work also for the neighbor Mimas. Mainly, it must be coherent with the absence of tectonic activity in Mimas, evidence of a much smaller dissipation. The results obtained with the theory developed in this paper are shown in Fig. 6.

The first result concerns the physical libration. Measurements of control points on the surface of Mimas accumulated over seven years of Cassini's observations allowed Tajeddine et al. (2014) to determine the satellite's rotation state. They found several libration components including one short-period oscillation of 50.3 ± 1 arcmin. If we assume that these oscillations follow a harmonic law, we obtain, correspondingly, for the oscillation of the velocity of rotation: 5.6 ± 0.1 deg/day, and for the semidiurnal frequency 11.2 ± 0.2 deg/day (see Tables 1 and 2). The comparison of these results to those shown in Fig. 6 (left) is that, like in the case of Enceladus, the observed value is larger than the tidal forced libration of Mimas (1.45 times) predicted by using a homogeneous body model. It is worth mentioning that this factor is not very different from the one obtained by Tajeddine et al. (2014) using models founded on the observed quadrupole moments of the gravitational potential of Mimas. In that case the relationship between the observed and the calculated amplitudes is 1.93 instead of 1.45 (compare with the 3.1 factor obtained in the case of Enceladus).

The absence of current tectonic activity in Mimas is evidence of a small dissipation. Figure 6 (right) shows that a small dissipation indicates that the relaxation factor γ of Mimas is much

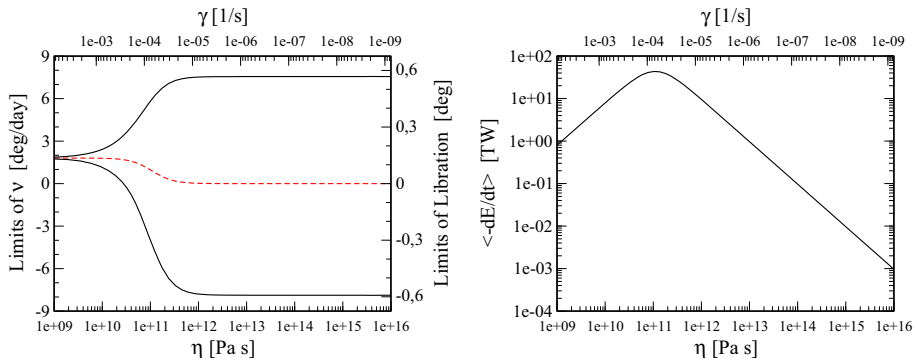


Fig. 6 Left: tidal forced oscillation of the semidiurnal frequency (and the corresponding limits of the physical libration) of one body like Mimas in function of the viscosity η and the relaxation factor γ (shown on the upper axis). The black lines are the limits of the oscillation and the red dashed line is the mean value of ν . Right: average of the net variation of the mechanical energy

Table 1 Satellites data used in the calculations

	Enceladus	Mimas
Mass (10^{20} kg)	1.08	0.379
Mean radius (km)	252.1	198.2
Sidereal period (d)	1.370218	0.942422
Semimajor axis (10^3 km)	238.02	185.52
Eccentricity	0.0045	0.01986
Mean motion (10^{-5} s $^{-1}$)	5.300508	7.696292

Table 2 Observed libration and dissipation and results of the homogeneous model

	Enceladus	Mimas
Observed		
Libration (deg)	0.120 ± 0.014	0.838 ± 0.002
Dissipation (GW)	5–16	–
Equatorial prolateness	$(2.0 \pm 0.2) \times 10^{-2}$	$(5.5 \pm 0.4) \times 10^{-2}$
Polar oblateness	$(2.2 \pm 0.1) \times 10^{-2}$	$(5.7 \pm 0.2) \times 10^{-2}$
Calculated		
Libration (deg)	0.039	0.589
Relaxation factor (s $^{-1}$)	$1.2\text{--}3.8 \times 10^{-7}$	$\sim 10^{-9}$ (*)
Viscosity (Pa s)	$0.6\text{--}1.9 \times 10^{14}$	$\sim 10^{16}$ (*)
Semimajor axis variation (km/y)	$-(0.6\text{--}1.8) \times 10^{-5}$	$\sim -10^{-6}$ (*)
Eccentricity variation (y $^{-1}$)	$-(1.9\text{--}6.0) \times 10^{-9}$	$\sim -10^{-10}$ (*)
Equatorial prolateness	2.34×10^{-2}	6.84×10^{-2}
Polar oblateness	1.95×10^{-2}	5.72×10^{-2}

(*) Assuming dissipation ~ 1 GW

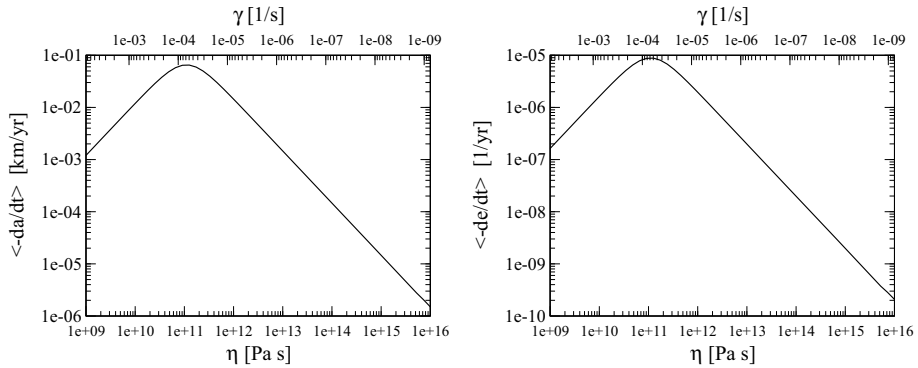


Fig. 7 Variation of the averages of $-da/dt$ (Left) and $-de/dt$ (Right) in function of the viscosity η (or γ , see the top axis) for a body like Mimas

smaller than that of Enceladus. Let us consider it as $\gamma \sim 10^{-9} \text{ s}^{-1}$ that corresponds to a dissipation smaller than 1 GW. The difference with the value found for Enceladus is surprising but it is consistent with the fact that the gravitational acceleration at the surface and the density are both much larger in Enceladus than in Mimas. Thus, the viscosity corresponding to the considered γ is $\sim 10^{16}$ Pa s, which is a reasonable value.

For the sake of completeness, we may add the results on the contribution of the satellite tides to the orbital evolution of Mimas. With the relaxation factor considered above, we obtain $\langle \dot{a}_{\text{sat}} \rangle \sim -10^{-6} \text{ km/y}$ and $\langle \dot{e}_{\text{sat}} \rangle \sim -10^{-10} \text{ y}^{-1}$ (Fig. 7). These variations are much smaller than those due to the tides on the planet. Anyway, the current eccentricity of Mimas cannot be explained by tidal effects alone and is rather related to the crossing of mean motion resonances in the past evolution of the satellite (Meyer and Wisdom 2008).

10 Conclusions

In this paper we propose an improved approach of the original creep tide theory. Supported by the analytical solutions given in the previous papers (papers I and II), we assume that the tidally deformed body has a triaxial ellipsoidal shape, where the flattenings and orientation are unknown functions of the time to be determined. The creep tide equation allows us to find the differential equations that describe the time evolution of this ellipsoidal bulge and its orientation, resulting in a very simpler and compact approach.

The other main result of the present investigation is the dissipation law and its application to quasi-synchronous homogeneous bodies discussed in Sects. 6 and 7. It is important to stress that the only hypothesis done in the theory is that the surface of the body permanently adjust itself to an equilibrium surface with speed given by the Newtonian creep law. No constitutive equation linking strain and stress is introduced at any point in the creep tide theory. All developments to reach the conclusion are the solution of the creep differential equation and the use of classical Physics to compute the force and torque acting on the external body due to the tidal deformation of the considered extended body. The observed dissipation law results directly from the above described first principles of Physics, with approximations but no additional ad hoc hypotheses.

In the case of Enceladus, used in this paper as example of application, the estimations of the heat dissipated in the SPT (south polar terrain) area based on the observations with

Cassini are in the range 5–16 GW (*cf* Howett et al. 2011; Spencer et al. 2013; Le Gall et al. 2017). In addition, a recent study by Kamata and Nimmo (2017) showed that a value about ten times higher than the old estimate of 1.1 GW is necessary if the ice shell is in thermal equilibrium. The given values correspond, using the creep tide theory, to a relaxation factor $\gamma = 1.2\text{--}3.8 \times 10^{-7} \text{ s}^{-1}$. The viscosity corresponding to this relaxation factor is $0.6\text{--}1.9 \times 10^{14} \text{ Pa s}$. It is of the same order as the value recently estimated by Efroimsky (2018) ($0.24 \times 10^{14} \text{ Pa s}$) and as the value adopted by Roberts and Nimmo (2008) for the viscosity of the ice shell ($10^{13} - 10^{14} \text{ Pa s}$). This value is also close to the reference viscosity of water at 255 K (10^{15} Pa s) adopted by Běhounková et al. (2012) in their modeling of the melting events at origin of the south-pole activity on Enceladus. More recent research carried out by Čadek et al. (2019) demonstrates that the viscosity of ice at the melting temperature is equal to or higher than $3 \times 10^{14} \text{ Pa s}$, for the ice shell to remain stable.

For this range of values of γ , we can calculate the variation of the semimajor axis (\dot{a}) = $-(0.4\text{--}1.3) \times 10^{-5} \text{ km/y}$. For the variation of the eccentricity, we obtained a very small value (\dot{e}) = $-(1.9\text{--}6.0) \times 10^{-9} \text{ y}^{-1}$. However, in the case of Enceladus, the effects of the almost 2:1 resonance between Enceladus and Dione produce a forced eccentricity of 0.00459 that must be considered (see Ferraz-Mello 1985; Vienne and Duriez 1995).

In contrast with Enceladus, the absence of current tectonic activity in Mimas is evidence of a small dissipation. A dissipation $\sim 1 \text{ GW}$ corresponds to a relaxation factor $\gamma \sim 10^{-9} \text{ s}^{-1}$ and a viscosity $\eta \sim 10^{16} \text{ Pa s}$, which are reasonable values. The difference with the values found for Enceladus is consistent with the fact that the gravitational acceleration at the surface and the density are both much larger in Enceladus than in Mimas. The different dissipations of Enceladus and Mimas may be simply associated with the fact that the outer layers of Enceladus have low viscosity (ice near the melting point) while Mimas with no tectonic activity due to internal heating has a viscosity at least one order of magnitude larger (ice at temperatures well below the melting point).

Rough models of heat conduction considering the known conductivity of the ice at low temperatures show that the crust ability to convey heat produced in the interior is of some 10^{-2} W/m^2 and can be larger or smaller than the values discussed in this paper, depending on the ice crust width and properties. The temperature measurements of the surface of Enceladus (Spencer et al. 2006) show that most of the internally produced heat is flowing through the faults existing in the SPT and this confirms the inability of the existing crust ice to fully convey the produced heat. This behavior is a clue for a non-stationary process in which an increase in temperature means a decrease in the viscosity and a larger dissipation. In Enceladus, such a process may have been triggered by some transitory event enhancing the eccentricity of Enceladus and may have been progressing slowly, subsisting even after the eccentricity was damped to its current value. The transient increase of the eccentricity may have happened at any moment because of the small distance separating the inner satellites of Saturn (see Nakajima et al. 2018).

Finally, measurements of control points on the surface of the satellites accumulated over seven years of Cassini's observations allowed Thomas et al. (2016) and Tajeddine et al. (2014) to determine their rotation state. They had found a libration of $0.120^\circ \pm 0.014^\circ$ for Enceladus and $50.3 \pm 1 \text{ arcmin}$ for Mimas. Assuming that these oscillations follow a harmonic law, we obtain, correspondingly, for the oscillation of the semidiurnal frequency $1.12 \pm 0.12 \text{ deg/day}$ for Enceladus and $11.2 \pm 0.2 \text{ deg/day}$ for Mimas. These observed values are larger than the tidal forced libration predicted by using a homogeneous body model (0.36 deg/day and 7.7 deg/day for Enceladus and Mimas, respectively). These disagreements between theory and observations are mainly due to the assumed homogeneity of the satellites. Indeed, the Enceladus libration can be obtained using a multilayered model (Folonier et al.,

in preparation), in which one liquid layer is assumed to exist between the crust and the core. All these results are summarized in Table 2.

The origin of the low dissipation value obtained in many papers using the classical models may be traced back to the use of Kelvin’s formula for k_2 and arbitrarily fixed values for the rigidity leading to $k_2 \leq 0.002$. If more realistic values of k_2 (and Q), are used, as those determined by Choblet et al. (2017, Supplement), the dissipation obtained with classical models is of the order of the observed values and coincide with the dissipation obtained in this paper when the viscosity is assumed to be that of melting ice. Efroimsky (2015, 2018) claims that for bodies of this kind, the rigidity plays virtually no role in tidal friction and k_2 is mainly defined by the viscosity of the body; thus, the use of Kelvin’s formula in such cases is not correct. The tide theory used in the present paper also considers the viscosity rather than the rigidity and the comparison of the approximate formulas established in Sect. 8.3 of this paper with the corresponding ones in classical theories gives, for synchronous stiff bodies, $k_2/Q \simeq 1.5\gamma/n = 0.75wR/n\eta$. This formula is virtually equivalent to the one relating k_2 and the viscosity given by Efroimsky (2018), with only a difference in the numerical factor.

Acknowledgements We thank Gwenaél Boué and Michael Efroimsky for their detailed reading of the original manuscript and for their enlightening suggestions. We also thank C. Beaugé and G.O. Gomes for several discussions. This investigation is funded by FAPESP, Grants 2016/20189-9, 2014/13407-4, 2016/13750-6 and 2017/10072-0, and by the National Research Council, CNPq, Grant 302742/2015-8. Preliminary results of this investigation were presented at the 9th Humboldt Colloquium on Celestial Mechanics, in Bad Hofgastein (Austria), March 2017.

Appendix 1: Gravitational energy of an ellipsoid. Results after Essén (2004)

The gravitational energy of an ellipsoid of mass m and semi-axes $a > b > c$ is explicitly given by

$$E_{\text{int}} = -\frac{3}{5} \frac{Gm^2}{R} X(\xi, \tau), \tag{40}$$

(Essén 2004) where the Taylor expansion of X around $\xi = 1, \tau = 0$ is

$$X(\xi, \tau) = 1 - \frac{4}{5}(\xi - 1)^2 - \frac{4}{15}\tau^2 + \dots, \tag{41}$$

and ξ, τ are functions of the flattening such that

$$a = (\xi + \tau)R; \quad b = (\xi - \tau)R; \quad c = (\xi^2 - \tau^2)^{-1}R. \tag{42}$$

Hence, to the first order,

$$\tau = \frac{1}{2}\mathcal{E}_\rho; \quad \xi - 1 = \frac{1}{3}\mathcal{E}_z, \tag{43}$$

and

$$E_{\text{int}} = -\frac{3}{5} \frac{Gm^2}{R} \left(1 - \frac{1}{15}\mathcal{E}_\rho^2 - \frac{4}{45}\mathcal{E}_z^2 \right). \tag{44}$$

The variation of the binding energy then is given by

$$\dot{E}_{\text{int}} = \frac{3}{5} \frac{Gm^2}{R} \left(\frac{2}{15}\mathcal{E}_\rho\dot{\mathcal{E}}_\rho + \frac{8}{45}\mathcal{E}_z\dot{\mathcal{E}}_z \right). \tag{45}$$

Equation (44) agrees with the result of the direct integration showing that the difference between the binding gravitational energy of an ellipsoid and that of the corresponding sphere is of the order of the square of the flattenings $\mathcal{E}_\rho, \mathcal{E}_z$.

It is worth mentioning that the alternative formulation due to Neusch (1979) does not agree neither with the results of Essén (2004) nor with the results of a direct integration.

Appendix 2: Near-synchronous analytical approximation

In order to find an analytical approximation to the instantaneous flattenings $\mathcal{E}_\rho, \mathcal{E}_z$, the rotation angle δ and the semidiurnal frequency $\nu = 2\Omega - 2n$ in the quasi-synchronous attractor, let us first consider a Keplerian motion for the companion M. Then, we consider the approximations:

$$\begin{aligned} \left(\frac{a}{r}\right)^3 &\approx 1 + \frac{3e^2}{2} + 3e \cos \ell \\ n - \dot{\phi} &\approx -2ne \cos \ell. \end{aligned} \tag{46}$$

Since, the rotation is quasi-synchronous, we may assume $\delta \ll 1$. Hence

$$\cos 2\delta \approx 1 - 2\delta^2; \quad \sin 2\delta \approx 2\delta. \tag{47}$$

Introducing these approximations into the creep tide and torque equations, (7) and (17) (using that $\nu = 2\Omega - 2n$, and $\dot{\nu} = 2\dot{\Omega}$) and neglecting the term $\dot{C}\Omega$, we obtain

$$\begin{aligned} \dot{\nu} &= -6\kappa n^2 \left(1 + \frac{3e^2}{2} + 3e \cos \ell\right) \mathcal{E}_\rho \delta \\ \dot{\delta} &= \frac{\nu}{2} - 2ne \cos \ell - \frac{\gamma \bar{\epsilon}_\rho}{\mathcal{E}_\rho} \left(1 + \frac{3e^2}{2} + 3e \cos \ell\right) \delta \\ \dot{\mathcal{E}}_\rho &= \gamma \bar{\epsilon}_\rho \left(1 + \frac{3e^2}{2} + 3e \cos \ell\right) (1 - 2\delta^2) - \gamma \mathcal{E}_\rho \\ \dot{\mathcal{E}}_z &= \frac{\gamma \bar{\epsilon}_\rho}{2} \left(1 + \frac{3e^2}{2} + 3e \cos \ell\right) + \gamma \bar{\epsilon}_z \frac{\Omega^2}{n^2} - \gamma \mathcal{E}_z, \end{aligned} \tag{48}$$

where $\kappa = M/(M + m)$, and

$$\bar{\epsilon}_\rho = \frac{15MR_e^3}{4ma^3}; \quad \bar{\epsilon}_z = \frac{5n^2 R_e^3}{4Gm}. \tag{49}$$

It is important to note that both $\bar{\epsilon}_\rho$ as $\bar{\epsilon}_z$ are constants.

Let us assume the particular solution

$$\begin{aligned} \nu &= B_0 + B_1 \cos \ell + B_2 \sin \ell \\ \delta &= D_0 + D_1 \cos \ell + D_2 \sin \ell \\ \mathcal{E}_\rho &= E_0 + E_1 \cos \ell + E_2 \sin \ell \\ \mathcal{E}_z &= Z_0 + Z_1 \cos \ell + Z_2 \sin \ell, \end{aligned} \tag{50}$$

the derivatives of which are

$$\begin{aligned}
 \dot{v} &= -nB_1 \sin \ell + nB_2 \cos \ell \\
 \dot{\delta} &= -nD_1 \sin \ell + nD_2 \cos \ell \\
 \dot{\mathcal{E}}_\rho &= -nE_1 \sin \ell + nE_2 \cos \ell \\
 \dot{\mathcal{E}}_z &= -nZ_1 \sin \ell + nZ_2 \cos \ell.
 \end{aligned}
 \tag{51}$$

Finally, replacing (50) and (51) into the system (48), collecting the terms with same trigonometric argument and neglecting terms of higher order, we obtain

$$\begin{aligned}
 B_0 &= \frac{12ne^2}{1+p^2} \frac{1+\alpha p^2}{1+\alpha^2 p^2} \\
 D_0 &= \frac{3pe^2}{1+p^2} \frac{2+(1+\alpha)p^2}{1+\alpha^2 p^2} \\
 E_0 &= \bar{\epsilon}_\rho \left(1 + \frac{3e^2}{2} - \frac{4p^2 e^2}{1+\alpha^2 p^2} \right) \\
 Z_0 &= \frac{\bar{\epsilon}_\rho}{2} \left(1 + \frac{3e^2}{2} \right) + \bar{\epsilon}_z \left(1 + \frac{12e^2}{1+p^2} \frac{1+\alpha p^2}{1+\alpha^2 p^2} + \frac{2(1-\alpha)^2 p^2 e^2}{1+\alpha^2 p^2} \right),
 \end{aligned}
 \tag{52}$$

and

$$\begin{aligned}
 \begin{pmatrix} B_1 \\ B_2 \end{pmatrix} &= \frac{12\kappa\bar{\epsilon}_\rho npe}{1+\alpha^2 p^2} \begin{pmatrix} -\alpha p \\ 1 \end{pmatrix} \\
 \begin{pmatrix} D_1 \\ D_2 \end{pmatrix} &= -\frac{2pe}{1+\alpha^2 p^2} \begin{pmatrix} 1 \\ \alpha p \end{pmatrix} \\
 \begin{pmatrix} E_1 \\ E_2 \end{pmatrix} &= \frac{3\bar{\epsilon}_\rho e}{1+p^2} \begin{pmatrix} 1 \\ p \end{pmatrix} \\
 \begin{pmatrix} Z_1 \\ Z_2 \end{pmatrix} &= \frac{1.5\bar{\epsilon}_\rho e}{1+p^2} \begin{pmatrix} 1 - \frac{16\kappa p^2 \bar{\epsilon}_z}{1+\alpha^2 p^2} \\ p + \frac{8\kappa p(1-\alpha^2 p^2)\bar{\epsilon}_z}{1+\alpha^2 p^2} \end{pmatrix},
 \end{aligned}
 \tag{53}$$

where $\alpha = 1 - 3\kappa\bar{\epsilon}_\rho$ and $p = n/\gamma$. We mention that the mean values B_0, D_0, E_0, Z_0 are given to the second order in eccentricity while the amplitudes B_i, D_i, E_i, Z_i ($i \neq 0$) are given to the first order in eccentricity.

Figure 8 shows the comparison of the near-synchronous attractors as given by the complete nonlinear system defined by Eqs. (7) and (17) and the approximate analytical solution given above in the case of one body like Enceladus, in function of the viscosity η . The dashed red lines show the maximum, minimum and mean values of $v, \delta, \mathcal{E}_\rho$ and \mathcal{E}_z (from top left to bottom right) given by the approximate solution, while the solid black lines show the maximum, minimum and the mean values of $v, \delta, \mathcal{E}_\rho$ and \mathcal{E}_z when the complete nonlinear system is integrated. The approximate solution is in excellent agreement with numerical integration of the equations.

Corrections to Paper II (Ferraz-Mello 2015)

1. Typo in Eq. (2). The right definition is $\epsilon_z = 1 - \frac{c_e}{R_e}$.

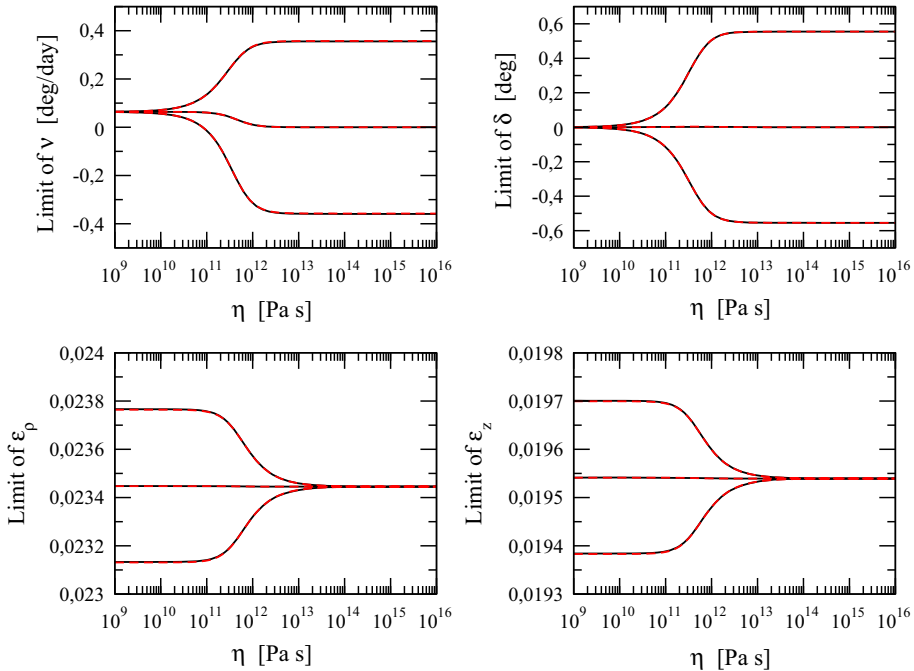


Fig. 8 Tidal forced oscillation of the semidiurnal frequency ν (top left), of the orientation angle of δ (top right), of the equatorial prolateness \mathcal{E}_ρ (bottom left) and of the polar oblateness \mathcal{E}_z (bottom right) of one body like Enceladus in function of the viscosity η . The black solid lines are the limits of the oscillations and the mean values given by the numerical integration of Eqs. (7) and (17). The red dashed lines are the limits of the oscillations and the mean values given by the analytical approximation given by Eqs. (50), (52) and (53)

2. In Eq. (16) the radial terms

$$\delta\zeta_{\text{rad}} = -\frac{1}{3}R \sum_{k \in \mathbb{Z}} C''_k \cos \bar{\sigma}''_k \cos(k\ell - \bar{\sigma}''_k)$$

are missing. (N.B. They are torqueless and conservative and do not affect the results.)

3. Typo in Eq. (31). The argument should be $k\ell - \bar{\sigma}''_k$.
4. Mistake in Eq. (61). In the last line the arguments should be $\nu + k\ell - \bar{\sigma}''_k$ and $\nu - k\ell + \bar{\sigma}''_k$.
5. Mistake in Eqs. (62–68) The sign in front of the zonal part is wrong. The sign in front of C''_k in Eqs. (62–63) should be +, the sign in front of $kE^2_{0,k}$ in Eqs. (64–66) should be –, and the sign in front of $knE^2_{0,k}$ in Eq. (68) should be +.
6. Typo in Eq. (69). The sign in front of the right-hand side should be changed to –.
7. Mistakes in Eq. (70). The correct equation is

$$\begin{aligned} \dot{e} = & -\frac{3GM_e R_e^2 \bar{\epsilon}_\rho}{10na^5 e} \sum_{k \in \mathbb{Z}} E_{2,k} \cos \bar{\sigma}_k \sum_{j \in \mathbb{Z}} \left(2\sqrt{1-e^2} - (2-k-j)(1-e^2) \right) E_{2,k+j} \sin(j\ell + \bar{\sigma}_k) \\ & - \frac{GM_e R_e^2}{10na^5 e} \sum_{k \in \mathbb{Z}} (\bar{\epsilon}_\rho E_{0,k} + 2\delta_{0,k} \bar{\epsilon}_z)(1-e^2) \cos \bar{\sigma}''_k \sum_{j \in \mathbb{Z}} (k+j) E_{0,k+j} \sin(j\ell + \bar{\sigma}''_k). \end{aligned}$$

8. Mistakes in Eq. (71). The correct equation is

$$\dot{e} = -\frac{3GM R_e^2 \bar{\epsilon}_\rho}{20na^5 e} \sum_{k \in \mathbb{Z}} \left(2\sqrt{1-e^2} - (2-k)(1-e^2) \right) E_{2,k}^2 \sin 2\bar{\sigma}_k \\ - \frac{GM R_e^2 \bar{\epsilon}_\rho}{20na^5 e} \sum_{k \in \mathbb{Z}} (1-e^2) k E_{0,k}^2 \sin 2\bar{\sigma}_k''.$$

9. Mistake in Eq. (B.6) (Online Supplement). The sign in front of $2\sqrt{1-e^2} E_{2,k}^{(5)}$ should be changed to $-$.

References

- Archinal, B.A., Acton, C.H., A'Hearn, M.F., Conrad, A.: Report of the IAU working group on cartographic coordinates and rotational elements: 2015. *Celest. Mech. Dyn. Astron.* **130**, 22 (2018)
- Běhounková, M., Tobie, G., Choblet, G., Čadek, O.: Tidally-induced melting events as the origin of south-pole activity on Enceladus. *Icarus* **219**, 655–664 (2012)
- Boué, G., Correia, A.C.M., Laskar, J.: Complete spin and orbital evolution of close-in bodies using a Maxwell viscoelastic rheology. *Celest. Mech. Dyn. Astron.* **126**, 31–60 (2016)
- Brouwer, D., Clemence, M.: *Methods of Celestial Mechanics*. Academic Press, New York (1961)
- Čadek, O., Souček, O., Běhounková, M., Choblet, G., Tobie, G., Hron, J.: Long-term stability of Enceladus' uneven ice shell. *Icarus* **319**, 476–484 (2019)
- Choblet, G., Tobie, G., Sotin, C., Běhounková, M., Čadek, O., Postberg, F., Souček, O.: Powering prolonged hydrothermal activity inside Enceladus. *Nat. Astron.* **1**, 841 (2017)
- Correia, A.C.M., Boué, G., Laskar, J., Rodríguez, A.: Deformation and tidal evolution of close-in planets and satellites using a Maxwell viscoelastic rheology. *Astron. Astrophys.* **571**, A50 (2014)
- Correia, A.C.M., Ragazzo, C., Ruiz, L.S.: The effects of deformation inertia (kinetic energy) in the orbital and spin evolution of close-in bodies. *Celest. Mech. Dyn. Astron.* **130**, 51 (2018)
- Darwin, G.H.: On the secular change in the elements of the orbit of a satellite revolving about a tidally distorted planet. *Philos. Trans.* **171**, 713–891 (1880). (repr. *Scientific Papers*, Cambridge, Vol. II, 1908)
- Efroimsky, M.: Tidal dissipation compared to seismic dissipation: in small bodies, earths, and super-earths. *Astrophys. J.* **746**, 150 (2012)
- Efroimsky, M.: Tidal evolution of asteroidal binaries. Ruled by viscosity. Ignorant of rigidity, *Astron. J.* **150**, 98 (2015) and Erratum: *Astron. J.* **151**, 130 (2016)
- Efroimsky, M.: Tidal viscosity of Enceladus. *Icarus* **300**, 223–226 (2018)
- Essén, H.: The physics of rotational flattening and the point core model. Preprint ArXiv 0403328v1, astro-ph.EP (2004)
- Ferraz-Mello, S.: First-order resonances in satellite orbits. In: Ferraz-Mello, S. (ed.) *Resonances in the Motion of Planets, Satellites and Asteroids*, IAG-USP, pp. 37–52. (1985)
- Ferraz-Mello, S.: Tidal synchronization of close-in satellites and exoplanets. A rheophysical approach. *Celest. Mech. Dyn. Astron.*, **116**, 109–140. (arXiv:1204.3957 astro-ph.EP) (paper I) (2013)
- Ferraz-Mello, S.: Tidal synchronization of close-in satellites and exoplanets: II. Spin dynamics and extension to Mercury and exoplanets host stars. *Celest. Mech. Dyn. Astron.* **122**, 359–389 (2015). (arXiv:1505.05384 astro-ph.EP) (paper II)
- Ferraz-Mello, S., Beaugé, C., Michtchenko, T.A.: Evolution of migrating planet pairs in resonance. *Celest. Mech. Dyn. Astron.* **87**, 99–112 (2003)
- Ferraz-Mello, S., Rodríguez, A., Hussmann, H.: Tidal friction in close-in satellites and exoplanets. The Darwin theory re-visited, *Celest. Mech. Dyn. Astron.*, **101**, 171–201 and Errata: *Celest. Mech. Dyn. Astron.* **104**, 319–320 (2009). (arXiv:0712.1156 astro-ph.EP) (2008)
- Folonier, H.A.: Tide on differentiated planetary satellites. Application to Titan. Ph.D. Thesis, IAG/University São Paulo (2016)
- Folonier, H.A., Ferraz-Mello, S.: Tidal synchronization of an anelastic multi-layered satellite. Titan's synchronous rotation. *Celest. Mech. Dyn. Astron.* **129**, 359–396 (2017). (arXiv:1706.08603 astro-ph.EP)
- Folonier, H.A., Ferraz-Mello, S., Kholshchevnikov, K.V.: The flattenings of the layers of rotating planets and satellites deformed by a tidal potential. *Celest. Mech. Dyn. Astron.* **122**, 183–198 (2015). (arXiv:1503.08051 astro-ph.EP)

- Frouard, J., Efroimsky, M.: Tides in a body librating about a spin-orbit resonance. Generalization of the Darwin-Kaula theory. *Celest. Mech. Dyn. Astron.* **129**, 177–214 (2017)
- Howett, C.J.A., Spencer, J.R., Pearl, J., Segura, M.: High heat flow from Enceladus' south polar region measured using 10–600 cm⁻¹ Cassini/CIRS data. *J. Geophys. Res. Planets* **116**, id. E03003 (2011)
- Jess, L., Stevenson, D.J., Parisi, M., Hemingway, D., Jacobson, R.A.: The gravity field and interior structure of Enceladus. *Science* **344**(6179), 78–80 (2014)
- Kamata, S., Nimmo, F.: Interior thermal state of Enceladus inferred from the viscoelastic state of the ice shell. *Icarus* **284**, 387–393 (2017)
- Kaula, W.M.: Tidal dissipation in the moon. *J. Geophys. Res.* **68**, 4959–4965 (1963)
- Kaula, W.M.: Tidal dissipation by solid friction and the resulting orbital evolution. *Rev. Geophys.* **3**, 661–685 (1964)
- Kopal, Z.: Gravitational heating of the moon. *Icarus* **1**, 412–421 (1963)
- Lainey, V., Karatekin, O., Desmars, J., Charnoz, S., Arlot, J.E., et al.: Strong tidal dissipation in Saturn and constraints on Enceladus thermal state from astrometry. *Astrophys. J.* **752**(1), 14 (2012)
- Le Gall, A., Leyrat, C., Janssen, M.A., Choblet, G., Tobie, G., et al.: Thermally anomalous features in the subsurface of Enceladus south polar terrain. *Nat. Astron.* **1**, 63 (2017)
- Lissauer, J.J., Stanton, J.P., Cuzzi, J.N.: Ring torque on Janus and the melting of Enceladus. *Icarus* **58**, 159–168 (1984)
- MacDonald, G.F.: Tidal friction. *Rev. Geophys.* **2**, 467–541 (1964)
- Meyer, J., Wisdom, J.: Tidal evolution of Mimas, Enceladus, and Dione. *Icarus* **193**, 213–223 (2008)
- Nakajima, A., Ida, S., Kimura, J., Brasser, R.: Orbital evolution of Saturn's mid-sized moons and the tidal heating of Enceladus. *Icarus* **317**, 570–582 (2018)
- Neusch, W.: On the gravitational energy of ellipsoidal bodies and some related functions. *Astron. Astrophys.* **72**, 339–347 (1979)
- Peale, S.J., Cassen, P.: Contribution of tidal dissipation to lunar thermal history. *Icarus* **36**, 245–269 (1978)
- Ragazzo, C., Ruiz, L.S.: Viscoelastic tides: models for use in Celestial Mechanics. *Celest. Mech. Dyn. Astron.* **128**, 19–59 (2017)
- Rambaux, N., Castillo-Rogez, J.C., Williams, J.G., Karatekin, Ö.: Librational response of Enceladus. *Geophys. Res. Lett.* **37**, L04202 (2010)
- Roberts, J.H., Nimmo, F.: Tidal heating and the long-term stability of a subsurface ocean on Enceladus. *Icarus* **194**, 675–689 (2008)
- Scheeres, D.J.: Stability in the full two-body problem. *Celest. Mech. Dyn. Astron.* **83**, 155–169 (2002)
- Segatz, M., Spohn, T., Ross, M.N., Schubert, G.: Tidal dissipation, surface heat flow, and figure of viscoelastic models of Io. *Icarus* **75**, 187–206 (1988)
- Shoji, D., Hussmann, H., Kurita, K., Sohl, F.: Ice rheology and tidal heating of Enceladus. *Icarus* **226**, 10–19 (2013)
- Spencer, J.R., Howett, C.J.A., Verbiscer, A., Hurford, T.A., Segura, M., Spencer, D.C.: Enceladus Heat flow from high spatial resolution thermal emission observations. *EPSC Abstr* **8**, EPSC2013-840-1 (2013)
- Spencer, J.R., Pearl, J.C., Segura, M., Flasar, F.M., Mamoutkine, A., Romani, P., Buratti, B.J., Hendrix, A.R., Spilker, L.J., Lopes, R.M.C.: Cassini encounters Enceladus: background and the discovery of a south polar hot spot. *Science* **311**, 1401–1405 (2006)
- Tajeddine, R., Rambaux, N., Lainey, V., Charnoz, S., et al.: Constraints on Mimas' interior from Cassini ISS libration measurements. *Science* **346**, 322–324 (2014)
- Thomas, P.C., Tajeddine, R., Tiscareno, M.S., Burns, J.A., Joseph, J., et al.: Enceladus's measured physical libration requires a global subsurface ocean. *Icarus* **264**, 37–47 (2016)
- Tisserand, F.: *Traité de Mécanique Céleste*, tome IV, chap. II. Gauthier-Villars, Paris (1891)
- Vienne, A., Duriez, L.: TASS 1.6: Ephemerides of the major Saturnian satellites. *Astron. Astrophys.* **297**, 588–605 (1995)
- Wisdom, J.: Tidal dissipation at arbitrary eccentricity and obliquity. *Icarus* **193**, 637–640 (2008)
- Yoder, C.F., Peale, S.J.: The tides of Io. *Icarus* **47**, 1–35 (1981)